Spatiotemporal controlled delivery of nanoparticles to injured vasculature

Juliana M. Chan[a], Liangfang Zhang[b], Rong Tong[c], Debuyati Ghosh[d], Weiwei Gao[e], Grace Liao[f], Kai P. Yuet[f], David Gray[d], June-Wha Rhee[e], Jianjun Cheng[c], Gershon Golomb[g], Peter Libby[h], Robert Langer[f,1], and Omid C. Farokhzad[e,1]

[a]Department of Biology, Massachusetts Institute of Technology, Cambridge, MA 02139; [b]Department of NanoEngineering, University of California at San Diego, La Jolla, CA 92093; [c]Department of Materials Science and Engineering, University of Illinois, Urbana, IL 61801; [d]Department of Materials Science and Engineering, Massachusetts Institute of Technology, Cambridge, MA 02139; [e]Laboratory of Nanomedicine and Biomaterials, Department of Anesthesiology, Brigham and Women's Hospital, Harvard Medical School, Boston, MA 02115; [f]Department of Chemical Engineering and Division of Health Science and Technology, Massachusetts Institute of Technology, Cambridge, MA 02139; [g]School of Pharmacy, Hebrew University, Jerusalem 91120, Israel; and [h]Division of Cardiovascular Medicine, Department of Medicine, Brigham and Women's Hospital, Boston, MA 02115

Contributed by Robert Langer, December 17, 2009 (sent for review November 9, 2009)

There are a number of challenges associated with designing nanoparticles for medical applications. We define two challenges here: (*i*) conventional targeting against up-regulated cell surface antigens is limited by heterogeneity in expression, and (*ii*) previous studies suggest that the optimal size of nanoparticles designed for systemic delivery is approximately 50–150 nm, yet this size range confers a high surface area-to-volume ratio, which results in fast diffusive drug release. Here, we achieve spatial control by biopanning a phage library to discover materials that target abundant vascular antigens exposed in disease. Next, we achieve temporal control by designing 60-nm hybrid nanoparticles with a lipid shell interface surrounding a polymer core, which is loaded with slow-eluting conjugates of paclitaxel for controlled ester hydrolysis and drug release over approximately 12 days. The nanoparticles inhibited human aortic smooth muscle cell proliferation in vitro and showed greater in vivo vascular retention during percutaneous angioplasty over nontargeted controls. This nanoparticle technology may potentially be used toward the treatment of injured vasculature, a clinical problem of primary importance.

peptides | collagen | nanoparticle | paclitaxel | angioplasty

The field of nanotechnology has crossed significant milestones from the systemic delivery of nanomedicines (1–5). However, the ability to achieve spatiotemporal control may be essential to many medical applications.

In this study, we engineer a nanoparticle (NP) system that fundamentally changes the way we control spatiotemporal delivery of therapeutic agents. We designed approximately 60-nm core-shell hybrid NPs (6, 7) consisting of a polymeric core, a lipid interface, and a poly(ethylene glycol) (PEG) corona. For temporal control, we achieved the capacity for slow drug elution over 2 weeks using poly(lactic acid) (PLA) conjugates of paclitaxel as a model therapeutic agent (8), made by a modified drug-alkoxide ring-opening strategy (9, 10). These conjugates allow for controlled drug release by gradual ester hydrolysis despite the large surface area and short diffusion distances of sub-100-nm particles. For spatial control, we functionalized our NPs with ligands (11, 12) that target across a range of diseases in a consistent and reproducible manner. Conventional molecular targeting of relevant cell-based targets can be confounded by inter- and intrapatient heterogeneity in cell surface antigen expression (13, 14). More recently, investigators have explored abundant noncellular targets such as the coagulation cascade (15), intraarticular cartilage (16), and extracellular matrix (17). Many human diseases are associated with compromised vasculature and increased vascular permeability (18, 19). Therefore, we exploit these vascular breaches by targeting the underlying basement membrane. Toward this goal, we screened for heptapeptide ligands by biopanning a phage library against collagen IV (20), which represents 50% of the vascular basement membrane (21), and characterized specific ligands for targeting affinity against a Matrigel extract rich in collagen IV and laminin (22).

We used angioplasty-injured vasculature as a model of compromised vasculature to examine the utility of our NPs. We delivered the targeted NPs via both intraarterial (IA) and i.v. administration and showed greater in vivo vascular retention at sites of injured vasculature in the rat compared to nontargeted NPs. Inspired by the adhesive nature of burr seeds, which are covered by "hooks" that bind onto abundant exposed surfaces, we named our system "nanoburrs" for their adhesive quality at sites of injured vasculature. The nanoburr system may be administered systemically for a myriad of human diseases where the endothelial lining is compromised, including oncologic (18) and cardiovascular inflammatory disease (18, 19, 23).

Results and Discussion

Selection and Characterization of Basement Membrane Targeting Peptides for Vascular Wall Targeting. To discover a functional vascular targeting peptide, a combinatorial library of random heptamers fused to the minor coat protein (pIII) of M13 filamentous phage was subjected to five rounds of biopanning against human collagen IV. Fifteen clones per round were randomly sequenced from Round 3–5 (R3–R5) (Fig. 1*A*), and in R5, 100% of the clones were found to be C-8, HWGSLRA. To find similarities to resident basement membrane structures, we searched the nonredundant version of the current National Center for Biotechnology Information *Homo sapiens* sequence database using the pBLAST algorithm against peptides from the screen (24, 25). Sequences were classified into three groups. The first group consists of peptides with homology to resident basement membrane proteins such as nidogen, serum amyloid P component, gelsolin, and laminin (21). The second group of peptides was enriched in proline residues, such as Pro-Pro-Ser (PPS) and Pro-Pro-Pro (PPP) runs, which resemble the Gly-Pro-Pro (GPP) motif in the collagen triple helix (20). Finally, the third group consists of unique peptides with no identifiable relationship with the basement membrane.

It has been discussed in the literature that penultimate rounds of biopanning may be a rich source of phage binders suspected to be lost due to reduced fitness (26). Possible reasons include reduced infectivity rates of phages for their *Escherichia coli* hosts due to low pH elution, disulfide-bond formation between cysteine containing phages resulting in the rarity of cysteine-rich

Author contributions: J.M.C., L.Z., G.G., P.L., R.L., and O.C.F. designed research; J.M.C., W.G., and G.L. performed research; R.T., D. Ghosh, K.P.Y., D. Gray, J.-W.R., and J.C. contributed new reagents/analytic tools; J.M.C. and O.C.F. analyzed data; and J.M.C. and O.C.F. wrote the paper.

The authors declare no conflict of interest.

[1]To whom correspondence may be addressed. E-mail: rlanger@mit.edu or ofarokhzad@zeus.bwh.harvard.edu.

This article contains supporting information online at www.pnas.org/cgi/content/full/0914585107/DCSupplemental.

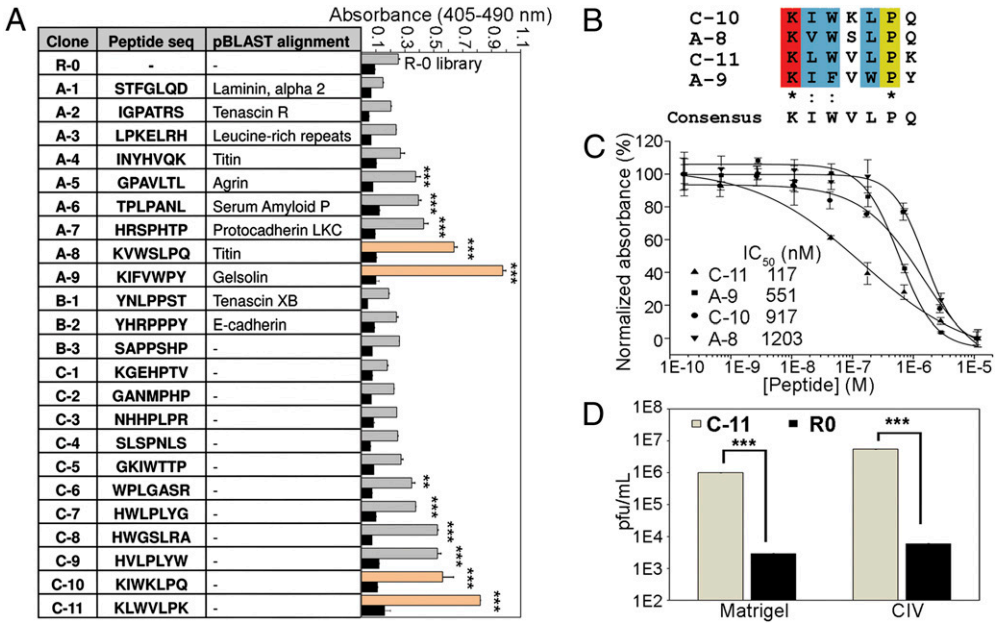

Fig. 1. Identification and characterization of peptides for targeting to injured vasculature. (*A*) Twenty-three phage clones from Rounds 3–5 of the phage display screen. Group A: Peptide sequences that show homology to resident basement membrane proteins or contain collagen binding-motifs analyzed by pBLAST against the NCBI *H. sapiens* nonredundant protein sequence database. Group B: Sequences that resemble the collagen IV GPP triple helix. Group C: Sequences with no identifiable relationship to resident basement membrane structures. The clones were tested against the library (R0) for binding to Matrigel (lighter shaded bars) and BSA (black bars). Bound phages were labeled with peroxidase-conjugated anti-M13 mAbs, and ABTS absorbance was read at 405 nm against a reference wavelength of 490 nm (mean ± SD, $n = 3$). **, $P < 0.01$; ***, $P < 0.001$, all compared with R0 (one-way analysis of variance with Tukey posthoc test). (*B*) Alignment and consensus sequence viewed using the CLUSTAL 2.0.10 multiple sequence alignment software. (*C*) Sequence-specific competition binding assays of phage clones A-8, A-9, C-10, and C-11 against synthetic peptide equivalents to Matrigel. IC_{50} values were determined and normalized on a percentage scale (mean ± SD, $n = 3$). (▲) C-11; (■) A-9; (●) C-10; (▼) A-8. (*D*) Titer count analyses of C-11 compared to R0 on Matrigel and collagen IV. Titers of eluted phages were averaged to give values of pfu/mL (mean ± SD, $n = 3$). ***, $P < 0.001$ by a paired two-sample Student's *t* test.

sequences, faster growth rates of certain clones, or simply a founder effect when a fraction of amplified phages are input into the next round of biopanning. In Fig. 1*A*, a binding experiment was performed to compare the affinities of the sequenced clones for Matrigel. 23 clones were incubated in triplicate against Matrigel (22) and BSA (*SI Materials and Methods*). The phages were ranked according to absorbance values indicating their binding capacity to Matrigel. No reactivity was observed against BSA compared with the random library (R0). Despite the similarity of the PP motifs with collagen IV, Group B peptides showed less binding affinity compared to Group A and C, and showed no detectable binding affinity above the library to Matrigel. Clones A-8, A-9, C-10, and C-11 were the best candidates, and we noted that these four clones resembled each other. The four clones were aligned pairwise using the CLUSTAL 2.0.10 multiple sequence alignment and gave a consensus sequence of KIWVLPQ, or more generally, KZWXLPX, where Z is a hydrophobic amino acid and X is any amino acid (Fig. 1*B*).

In a sequence-specific competition assay, we analyzed the context-dependence of the phage toward the peptide-collagen IV binding interaction (*SI Materials and Methods*). Synthetic peptides modeled after phage clones A-8, A-9, C-10, and C-11 competitively inhibited their cognate phage in a dose-dependent manner on Matrigel-coated surfaces (Fig. 1*C*). Phage C-11 showed the best peptide competition, which suggests that C-11 binding affinity may represent a specific peptide-collagen IV interaction independent of the phage context. We further examined the binding of phage C-11 in three independent titer count analyses (Fig. 1*D*). Phage titers of C-11 were compared against the library (R0) for binding to Matrigel and collagen IV with an initial phage input of 10^{12}/mL pfu. C-11 showed approximately 300-fold Matrigel binding and approximately 900-fold collagen IV binding compared to the library ($n = 3$, $P < 0.001$).

Synthesis and Characterization of the Nanoburr Drug Delivery System. To investigate the targeting properties of the candidate peptide against the basement membrane, we covalently conjugated peptides onto hybrid NPs that have a hydrophobic drug-eluting core, a hydrophilic polymeric shell, and a lipid monolayer (7). PEG (1) covalently conjugated to 1,2-distearoyl-sn-glycero-3-phosphoethanolamine (DSPE) was used to form the hydrophilic polymeric shell. To complete the lipid monlayer, soybean lecithin, which is considered Generally Regarded as Safe (GRAS), was used to form the core-shell interface. For the hydrophobic drug-eluting core, we synthesized paclitaxel–polylactide (Ptxl–PLA) conjugates by a drug/alkoxide-initiated ring-opening polymerization strategy (10). Ptxl was mixed with equimolar amounts of [(BDI)ZnN(TMS)$_2$] [BDI =2-((2,6-diisopropylphenyl)amino)-4-((2,6-diisopropylphenyl)imino)-2-pentene, TMS = trimethylsilyl] (9), and the (BDI)Zn–Ptxl complex formed in situ subsequently initiated and completed the polymerization of lactide within hours at room temperature (Fig. 2*A*). Ptxl was shown to be conjugated to the terminals of PLA by comparing the elution profile of free Ptxl to Ptxl–PLA by reverse phase-high performance liquid chromatography (RP-HPLC) (*SI Materials and Methods*). Ptxl–PLA eluted at approximately 21 min instead of eluting at the original approximately 14 min Ptxl peak (Fig. 2*B*).

In Fig. 2*C*, nanoburr synthesis is illustrated in which the core (Ptxl–PLA conjugate) and shell (lipid and lipid–PEG) are integrated via nanoprecipitation and self-assembly. We conjugated the KLWVLPK peptide via a C-terminal GGGC linker to DSPE-PEG-maleimide using maleimide-thiol conjugation chemistry. Transmission electron microscopy (TEM) showed the spherical structures of nanoburrs (Fig. 2*D*). The size and surface zeta potential of nonfunctionalized NPs in water were 57.3 ± 0.4 nm (mean ± SD) (Fig. 2*E*) and −12.83 ± 2.73 mV (mean ± SD) (Fig. 2*F*), respectively. Peptide attachment resulted in an approximately 1-nm size

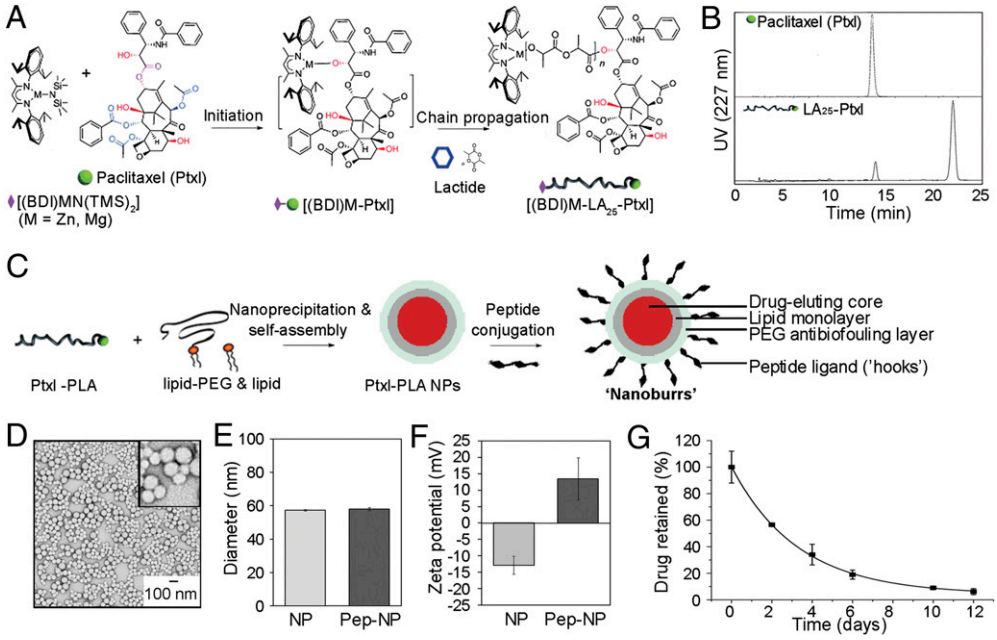

Fig. 2. Nanoburr core-shell synthesis and characterization. (*A*) Schematic of Ptxl–PLA biomaterial synthesis. Ptxl was mixed with equimolar amounts of [(BDI)ZnN(TMS)$_2$]; the (BDI)Zn–Ptxl complex formed in situ initiated and completed the polymerization of lactide. For the nanoburr core, we synthesized Ptxl–PLA$_{25}$ drug conjugates, which have approximately 25 D,L-lactide monomer units. (*B*) RP-HPLC analysis of Ptxl against Ptxl–PLA$_{25}$ conjugates. (*C*) Schematic of nanoburr synthesis by nanoprecipitation and self-assembly. Ptxl–PLA in acetone was added dropwise to a heated lipid solution, vortexed vigorously, and allowed to self-assemble for 2 h to form NPs. The NPs were peptide-functionalized using maleimide-thiol chemistry. Nanoburrs have a drug-eluting polymeric core, a lipid monolayer, a PEG antibiofouling layer, and peptide ligands (hooks) to adhere to the exposed basement membrane during vascular injury. (*D*) TEM image of nanoburrs stained with 3% uranyl acetate. (Scale bar, 100 nm.) (*E*) Dynamic light scattering measurements before and after peptide conjugation, respectively. (*F*) Zeta potential measurements before and after peptide conjugation, respectively. (*G*) In vitro drug release of Ptxl from the nanoburr core. Samples at different time points were measured for absorbance at 227 nm (mean ± SD, n = 3).

increase and made the surface charge cationic (13.5 ± 5.9 mV, mean ± SD), presumably because the peptides were N-terminally exposed to retain their original phage-displayed orientation.

To characterize the nanoburrs physiochemically, we quantified their release kinetics by taking aliquots (n = 3) at scheduled time points for RP-HPLC analysis (Fig. 2*G*). Ptxl is released by diffusion when the Ptxl–PLA ester bond is hydrolyzed, and the amount of Ptxl released from Ptxl–LA$_{25}$ was 43.4% on day 2, and 91.0% and 93.8% on day 10 and day 12, respectively. Drug elution rates can be further controlled by varying lactide/Ptxl ratios during ring-opening polymerization, resulting in different PLA chain lengths attached to the Ptxl drug (8). The use of polymers to control Ptxl release is also a significant feature of drug eluting stents (DES), however, 80–90% of the Ptxl fraction is never released (27).

The two parameters of drug loading and release are important for drug efficacy. Increased drug loading into the particle core tends to reduce overall stability, giving an undesired burst release effect and reduced efficacy (28). Larger particles tend to have slower in vitro release profiles, but when systemically delivered may be more readily detected and cleared from circulation, resulting in a lack of efficacy (29). For vascular targeting, because small particles show improved vessel adhesion and retention (16, 30–32), integrating slow-eluting conjugates into the nanoburr design allows for (*i*) improved drug loading; (*ii*) sub-100-nm NPs for vascular targeting; and (*iii*) sustained drug release over 2 weeks.

Targeted Drug Release from Nanoburrs. To validate the therapeutic efficacy of this treatment, a human aortic smooth muscle cell (haSMC) cytotoxicity study was used to assess nanoburr differential cellular cytotoxicity and binding affinity on Matrigel-coated wells with haSMC (Fig. 3). To test the sequence specificity of the KLWVLPK peptide (T), we designated two controls: scrambled PWKKLLV peptide (S) and nontargeted (B) NPs. In addition, we included a media-only control and fourfold dilutions of free Ptxl in DMSO (maximum 0.1% DMSO in media). The maximum free

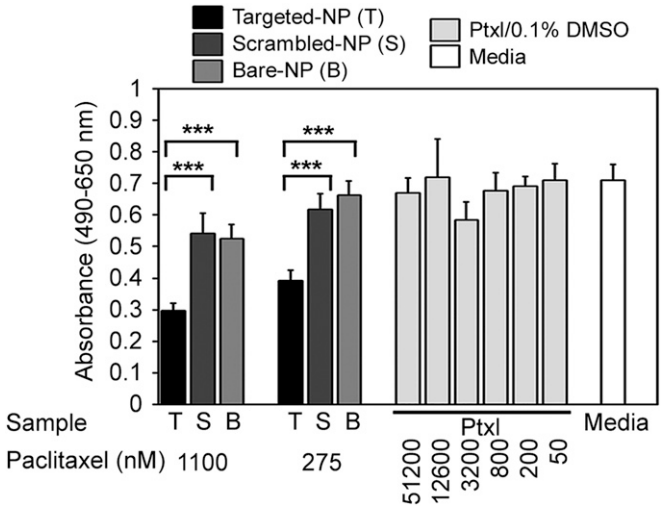

Fig. 3. Targeted drug release from nanoburrs. haSMC cytotoxicity studies as a function of binding affinity; haSMC on Matrigel-coated plates were incubated with nanoburrs (T), scrambled-NPs (S), nontargeted bare-NPs (B), 4-fold dilutions of Ptxl, and a media-only control for 45 min. Samples were washed two times in complete media and replaced with fresh media for 48 h. Formazan product formation was measured at 490 nm against a reference wavelength of 650 nm (mean ± SD, n = 5). ***, $P < 0.001$ by one-way analysis of variance with Tukey post hoc test.

Ptxl concentration used was 51 μM, exceeding by two log scales a suitable Ptxl dose range of 50–1,000 nM for haSMC cytotoxicity. An incubation time of 45 min was significantly shorter than typical incubation times with Ptxl (approximately 4–24 h). The wells were rinsed twice with complete media and further incubated with fresh media for 48 h. Unlike free Ptxl, which is removed during the washing step, the nanoburrs attached to the collagen IV matrix were retained for continued Ptxl release. Hence, lowered formazan product formation (absorbance at 490 nm) reflects increased haSMC cytotoxicity as a function of greater targeted-NP retention on Matrigel-coated plates ($n = 5$, $P < 0.001$).

Binding Studies in Angioplasty Models of Injured Vasculature. We evaluated the targeting affinity of the nanoburr system toward injured vasculature. To create those vascular characteristics, a Fogarty 2-French balloon catheter was used to injure rat arteries by repeatedly advancing, inflating the balloon, and withdrawing to denude the endothelial monolayer and expose the basement membrane. This loosely mimics a percutaneous angioplasty procedure in human patients, the difference being that in human patients the catheter is inflated locally in a preexisting stenotic lesion. In Fig. 4*A*, a representative H&E stained cross-section shows an injured aorta with the endothelial layer removed, and an uninjured aorta with an intact endothelial monolayer.

Our ex vivo study examined targeting of the nanoburr system to balloon-injured rat aortas. We used Alexa Fluor 647 fluorescent dye-poly(lactic-*co*-glycolic acid) (A647–PLGA) conjugates as a substitute for Ptxl–PLA drug conjugates to visualize the nanoburrs by fluorescence microscopy and optical imaging. This wavelength is beyond the autofluorescence range of typical endogenous tissue fluorophores such as collagen and elastin, which excite and emit maximally at approximately 300–500 nm. Therefore, any A647–PLGA fluorescence detected would be NP deposition. A647–PLGA encapsulated nanoburrs were incubated in the abdominal aorta for 5 min under constant pressure, followed by extensive washing using a syringe-pump to remove nonadsorbed samples (Fig. 4*B*). Subsequently, the abdominal aortas were harvested and viewed by whole vessel fluorescent optical imaging (*SI Materials and Methods*). In fluorescent imaging, the detected surface intensity depends on the illumination intensity, which varies according to the field-of-view and wavelength. To eliminate the effect of illumination intensity, images are normalized against a reference illumination image. The resulting "normalized" fluorescent efficiency image is unitless, and the value of each pixel represents the fractional ratio of emitted photons per incident excitation photon. We used the region-of-interest (ROI) function to quantify nanoburr retention (Fig. S1), and measurements are displayed as average fluorescent efficiency (relative fluorescence units, rfu). The nanoburrs bound to balloon-injured aortas (Fig. 4*C*) at $1.43 \pm 0.48 \times 10^{-4}$ (rfu), while scrambled-peptide and nontargeted NPs bound on average twofold less at 48% ($n = 3$, $P < 0.05$) and 47% ($n = 3$, $P < 0.05$), respectively. To ensure that the nanoburrs would not target intact endothelial layers, they were also incubated with uninjured aortas and bound fourfold less at $3.39 \pm 0.50 \times 10^{-5}$ (rfu) ($n = 3, P < 0.01$) compared to injured vessels. Frozen histological sections were photographed to show nanoburr binding along the arterial cross-section (Fig. S2).

We next examined targeting in vivo via IA infusion using a left carotid injury model (Fig. 4*D*). The nanoburrs were injected into angioplastied left carotids through a catheter positioned in the aortic arch over the course of 1 min and allowed to circulate for 1 h. Fourfold more nanoburrs [$8.71 \pm 0.38 \times 10^{-6}$ (rfu)] were found in

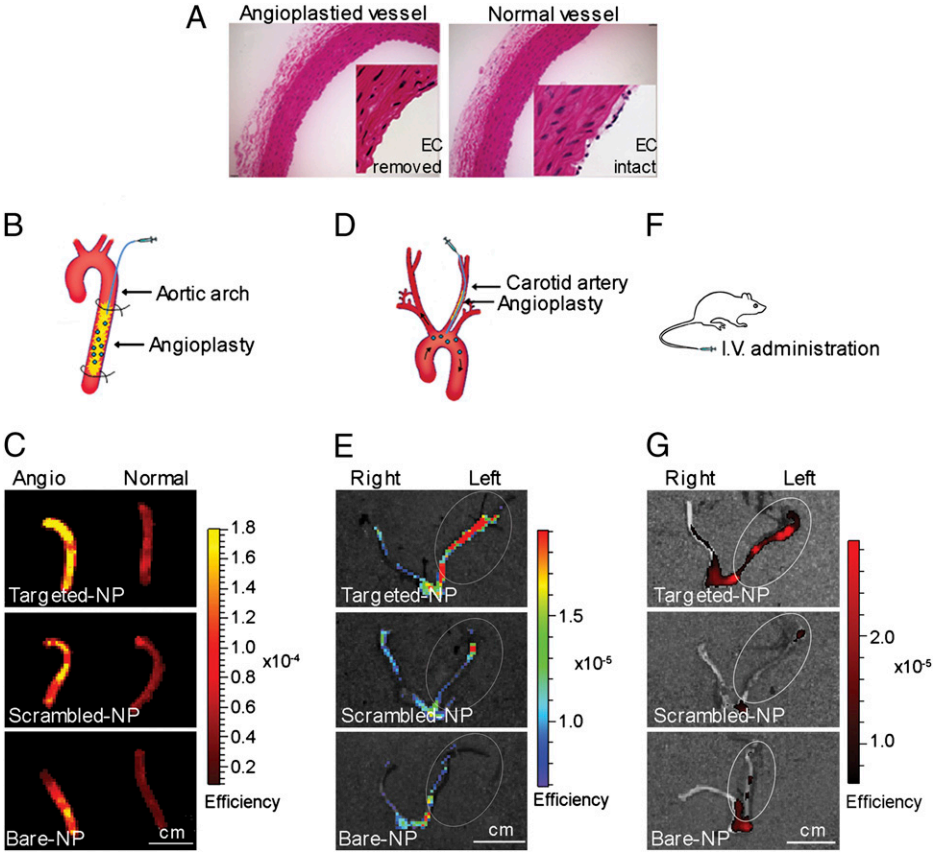

Fig. 4. Nanoburr targeting in angioplasty models of injured vasculature. (*A*) Representative H&E stained cross-sections of balloon-injured and uninjured aortas. Balloon-injury removes the endothelial cell (EC) monolayer. (*B*) Ex vivo delivery in an abdominal aorta injury model. Samples were delivered into the aorta segment for 5 min in situ. Nonadsorbed samples were flushed out by saline infusion for 15 min. (*C*) Fluorescence images overlayed on photographs of balloon-injured aortas incubated with nanoburrs, compared with scrambled-peptide and nontargeted NPs. (*D*) In vivo IA delivery in a carotid injury model. A catheter was inserted via the external carotid into the common carotid and advanced into the aortic arch. Samples were delivered at 1 mL/min for 1 min and allowed to circulate for 1 h before the animals were killed. (*E*) Fluorescence images overlayed on photographs of carotid arteries incubated with nanoburrs, compared with scrambled-peptide and nontargeted NPs. (*F*) In vivo systemic delivery in a carotid angioplasty model. Samples were delivered by 1 mL i.v. tail vein injection and allowed to circulate for 1 h before the animals were killed. (*G*) Fluorescence images overlayed on photographs of carotid arteries incubated with nanoburrs, compared with scrambled-peptide and nontargeted NPs. For imaging, Alexa Fluor 647–PLGA dye conjugates were encapsulated in place of Ptxl–PLA drug conjugates. (Scale bar, 1 cm.)

the angioplastied left carotid arteries compared to healthy right carotids (Fig. 4*E*). Scrambled-peptide and nontargeted NPs were retained in the left carotids at 40% ($n = 3, P = 0.0818$) and 53% ($n = 3, P = 0.23716$) of nanoburr retention, respectively (Fig. S3). Representative frozen histological sections show fluorescence along the carotid arteries (Fig. S4).

The nanoburr system was studied for systemic delivery because repeat dosing may be helpful in the treatment of chronic vascular disease (30). Using a left carotid injury model, the nanoburrs were given as a 1 mL i.v. dose via tail-vein injection and allowed to circulate for 1 h (Fig. 4*F*). Nanoburr retention was $5.46 \pm 1.02 \times 10^{-6}$ (rfu) in the angioplastied left carotids compared to scrambled-peptide and nontargeted NPs (Fig. 4*G*), which were 35% ($n = 5, P < 0.001$) and 64% ($n = 5, P < 0.01$) of nanoburr retention, respectively. The nanoburrs bound to the left carotids twofold over healthy right carotids ($P < 0.001$) (Fig. S5). Representative fluorescence images of nanoburr binding are shown in Fig. S6.

Our binding studies to sites of injured vasculature altogether show the successful targeting and retention of nanoburrs to injured carotid arteries in vivo and abdominal aortas ex vivo. Further in vivo tests of efficacy are necessary to expand on our findings.

Conclusion

In summary, we developed a spatiotemporally controlled delivery vehicle using clinically safe biomaterials that have the capacity to target injured vasculature. When these vehicles are administered IA or i.v., they demonstrate localization to sites of injured vasculature and exhibit controlled drug release over approximately 10–12 days in vitro. Our initial application of this technology was for vessel wall targeting in cardiovascular disease. The utility of the nanoburr system is broader and may include oncologic and regenerative diseases and indications where neoangiogenesis is commonly observed.

Materials and Methods

A detailed description of materials and methods is available in *SI Materials and Methods*.

Screening of Phage Display Peptide Library. The Ph.D.-7 phage library was obtained from New England Biolabs. Briefly, approximately 10 μg/mL human collagen IV in 0.1 M $NaHCO_3$, pH 8.6 was coated onto a 96-well enzyme and radioimmunoassay (EIA/RIA) high binding plate (Corning Life Sciences) overnight at 4 °C for biopanning according to the manufacturer's instructions. From R2 to R5, the Tween-20 concentration was raised to 0.5%, and the collagen IV enriched phage pool from R1 was subtractively panned against human collagen I for 1 h at room temperature (RT) to reduce collagen I binding interference before biopanning against collagen IV. In R5, 1-μg/mL collagen IV coated plates were used for increased stringency. Fifteen clones per round were randomly picked from R3 to R5 for DNA sequencing and further analysis (*SI Materials and Methods*).

Paclitaxel-Polylactide Conjugation. [(BDI)ZnN(TMS)$_2$] [(BDI =2-((2,6-diisopropylphenyl)amino)-4-((2,6-diisopropylphenyl)imino)-2-pentene, TMS = trimethylsilyl] (6.2 mg, 0.01 mmol) and Ptxl (8.5 mg, 0.01 mmol) were mixed in 0.5-mL anhydrous THF. D,L-Lactide (36 mg, 0.25 mmol) in 2 mL anhydrous THF was added dropwise to initiate polymerization. Lactide was completely consumed within hours at RT and monitored by FTIR or ^{1}H NMR spectroscopy. The polymerization solution was added to ethyl ether (25 mL) to precipitate out the Ptxl–PLA$_{25}$ conjugate (approximately 25 dL-lactide monomer units, 19.2 wt% Ptxl).

Synthesis and Characterization of Nanoburrs. A 3-mL DSPE-PEG/lecithin mixture in 4% ethanol containing 0.17 mg DSPE-PEG-Maleimide/DSPE-PEG (1:4 molar ratio) and 0.08 mg lecithin was heated for 3 min above the lipid phase transition temperature to 68 °C under gentle stirring. After heating, 1 mg of Ptxl–PLA in acetone (1 mg/mL) was added dropwise at 1 mL/min. The solution was vortexed vigorously for 3 min followed by self-assembly under gentle stirring for 2 h at RT. The NPs were washed three times using an Amicon Ultra-4 centrifugal filter with 30,000 Da MWCO (Millipore). The NPs were resuspended in pH 7.2 PBS buffer and 2 mM EDTA and incubated with peptides (MW = 1137.54 Da) at a 1/2 molar ratio to DSPE-PEG-Mal for 45 min at RT. The peptides were previously reduced using Bond-breaker TCEP solution, Neutral pH (Thermo Scientific) in PBS-EDTA at a 1/1 disulfide bond/TCEP molar ratio. Free peptides were removed using a Sephadex PD-10 (G-25) column. For scale-up, multiple vials of NPs were made with concentrations and volumes kept constant to maintain small NP diameters. For animal studies, NPs were sterile filtered before IA or i.v. delivery. TEM images of the nanoburrs (1 mg/mL) were obtained by negative-staining with 3% uranyl acetate. Size (diameter, nm) and surface charge (zeta potential, mV) were evaluated by quasi-elastic laser light scattering using a ZetaPALS dynamic light-scattering detector (15 mW laser, incident beam = 676 nm; Brookhaven Instruments).

haSMC Cytotoxicity Studies. Ninety-six-well plates were Matrigel-coated and BSA-blocked (as described in *SI Materials and Methods*) in PBS. HaSMC were plated at 10,000 cells/well in a 37 °C/5% CO_2 incubator and grown for 24 h in Medium 231 supplemented with 10 μg/mL gentamycin, 0.25 μg/mL amphotericin B, and smooth muscle growth supplement (all from Cascade Biologics, Invitrogen). Treatment groups ($n = 5$) included nanoburrs, scrambled-peptide NPs, nontargeted NPs, fourfold dilutions of Ptxl (in maximum 0.1% DMSO) in media and a media-only control. Samples were incubated with cells for 45 min. The wells were washed two times with complete media and replaced with fresh complete media for 48 h. Medium 231 was replaced with phenol red-free RPMI medium supplemented with 10% FBS (Invitrogen) containing [3-(4,5-dimethylthiazol-2-yl)-5-(3-carboxymethoxyphenyl)-2-(4-sulfophenyl)-2H-tetrazolium, inner salt] (MTS) and phenazine methosulfate (PMS) and incubated for 2 h at 37 °C (CellTiter 96 AQ_{ueous} Non-Radioactive Cell Proliferation Assay; Promega). Formazan product formation was measured by absorbance at 490 nm against a reference wavelength of 650 nm.

Balloon-Angioplasty ex Vivo and in Vivo Studies. Sprague–Dawley rats weighing approximately 450–500 g were obtained from Charles River Laboratories and fed a normal rodent diet. All animal procedures were conducted by a certified contract research organization using protocols consistent with local, state, and federal regulations as applicable and approved by the Institutional Animal Care and Use Committee.

For ex vivo studies, animals were killed for open abdominal cavity surgery in situ. Aortas were flushed with saline and injured by four passages of a Fogarty arterial embolectomy 2F balloon catheter (Model 120602F; Edwards Lifesciences) in a rotating fashion. AlexaFluor 647 (A647) dyes were covalently conjugated to PLGA (viscosity 0.19 dL/g) using EDC/NHS chemistry in DMF. A647–PLGA conjugates were precipitated in 2/1 ethyl ether/methanol by centrifugation, dried in vacuum, and resuspended in acetone for NP preparation. Fluorescence (rfu) was quantified using a GeminiXPS microplate spectrofluorometer (Molecular Devices), and samples were diluted accordingly in PBS for comparable NP delivery into the aortas. 0.4-mL samples (approximately 6 mg/mL) were incubated in the aorta for 5 min using metal clips to secure both ends of the aorta. Nonadsorbed samples were flushed away with saline using an Advance Infusion Pump Series 1200 syringe pump (Roboz Surgical Instrument Co.) programmed at 4 mL/min for 15 min.

For in vivo IA studies, animals were anesthetized intramuscularly with ketamine (60 mg/kg)/kylzaine (10 mg/kg) and given buprenorphine as an analgesic. Left common carotids were injured by four passages of the 2F balloon-catheter, before a 30-gauge tubing was inserted via the external carotid into the common carotid and advanced beyond the angioplastied region into the aortic arch. Samples (approximately 10 mg/mL) were infused at 1 mL/min for 1 min. The external carotids were permanently ligated. The animals were killed 1 h after surgery, and the carotids were harvested.

For in vivo i.v. studies, animals were additionally given heparin (500 IU/kg) by i.v. injection immediately before surgery. The animals underwent left common carotid artery surgery and samples (approximately 15 mg/mL) were given by 1-mL i.v. tail vein injections. The animals were killed after 1 h and the carotids were harvested.

ACKNOWLEDGMENTS. We thank Angelia Doye, Juan Deleon, and Dr. Judith Gwathmey for their assistance with the animal surgeries. We thank Dr. Elazer Edelman and Dr. Chester Drum for helpful discussions. We thank Dr. Richard Cook and Natalia Schiller of the Massachusetts Institute of Technology Biopolymers Laboratory and the Koch Institute Microscopy and Imaging Core Facility. This work was supported by National Institutes of Health Grants CA119349 and EB003647; and the Koch–Prostate Cancer Foundation Award in Nanotherapeutics. J.M.C. acknowledges the financial support from the B.S.-Ph.D. National Science Scholarship awarded by the Agency for Science, Technology and Research, Singapore.

1. Gref R, et al. (1994) Biodegradable long-circulating polymeric nanospheres. *Science* 263:1600–1603.
2. Zhang L, et al. (2008) Nanoparticles in medicine: Therapeutic applications and developments. *Clin Pharmacol Ther* 83:761–769.
3. Kim TY, et al. (2004) Phase I and pharmacokinetic study of Genexol-PM, a cremophor-free, polymeric micelle-formulated paclitaxel, in patients with advanced malignancies. *Clin Cancer Res* 10:3708–3716.
4. Davis ME, Chen ZG, Shin DM (2008) Nanoparticle therapeutics: An emerging treatment modality for cancer. *Nat Rev Drug Discov* 7:771–782.
5. Nel AE, et al. (2009) Understanding biophysicochemical interactions at the nano-bio interface. *Nat Mater* 8:543–557.
6. Zhang L, et al. (2008) Self-assembled lipid—polymer hybrid nanoparticles: A robust drug delivery platform. *ACS Nano* 2:1696–1702.
7. Chan JM, et al. (2009) PLGA-lecithin-PEG core-shell nanoparticles for controlled drug delivery. *Biomaterials* 30:1627–1634.
8. Tong R, Cheng J (2008) Paclitaxel-initiated, controlled polymerization of lactide for the formulation of polymeric nanoparticulate delivery vehicles. *Angew Chem Int Ed Engl* 47:4830–4834.
9. Chamberlain BM, et al. (2001) Polymerization of lactide with zinc and magnesium beta-diiminate complexes: Stereocontrol and mechanism. *J Am Chem Soc* 123:3229–3238.
10. Dechy-Cabaret O, Martin-Vaca B, Bourissou D (2004) Controlled ring-opening polymerization of lactide and glycolide. *Chem Rev* 104:6147–6176.
11. Peer D, et al. (2007) Nanocarriers as an emerging platform for cancer therapy. *Nat Nanotechnol* 2:751–760.
12. Langer R (1998) Drug delivery and targeting. *Nature* 392:5–10.
13. Rajan P, Elliott DJ, Robson CN, Leung HY (2009) Alternative splicing and biological heterogeneity in prostate cancer. *Nat Rev Urol* 6:454–460.
14. Andrechek ER, et al. (2009) Genetic heterogeneity of Myc-induced mammary tumors reflecting diverse phenotypes including metastatic potential. *Proc Natl Acad Sci USA* 106:16387–16392.
15. Peters D, et al. (2009) Targeting atherosclerosis by using modular, multifunctional micelles. *Proc Natl Acad Sci USA* 106:9815–9819.
16. Rothenfluh DA, Bermudez H, O'Neil CP, Hubbell JA (2008) Biofunctional polymer nanoparticles for intra-articular targeting and retention in cartilage. *Nat Mater* 7: 248–254.
17. O'Neil CP, et al. (2009) Extracellular matrix binding mixed micelles for drug delivery applications. *J Control Release* 137:146–151.
18. Folkman J (2007) Angiogenesis: An organizing principle for drug discovery? *Nat Rev Drug Discov* 6:273–286.
19. Ross R (1999) Atherosclerosis—an inflammatory disease. *N Engl J Med* 340:115–126.
20. Hudson BG, Reeders ST, Tryggvason K (1993) Type IV collagen: Structure, gene organization, and role in human diseases. Molecular basis of Goodpasture and Alport syndromes and diffuse leiomyomatosis. *J Biol Chem* 268:26033–26036.
21. Kalluri R (2003) Basement membranes: Structure, assembly and role in tumour angiogenesis. *Nat Rev Cancer* 3:422–433.
22. Kleinman HK, et al. (1982) Isolation and characterization of type IV procollagen, laminin, and heparan sulfate proteoglycan from the EHS sarcoma. *Biochemistry* 21: 6188–6193.
23. Libby P (2002) Inflammation in atherosclerosis. *Nature* 420:868–874.
24. Altschul SF, et al. (1997) Gapped BLAST and PSI-BLAST: A new generation of protein database search programs. *Nucleic Acids Res* 25:3389–3402.
25. Schäffer AA, et al. (2001) Improving the accuracy of PSI-BLAST protein database searches with composition-based statistics and other refinements. *Nucleic Acids Res* 29:2994–3005.
26. Smith GP, Petrenko VA (1997) Phage Display. *Chem Rev* 97:391–410.
27. Grube E, et al. (2006) Evaluation of a new polymer-coated paclitaxel-eluting stent for treatment of de novo lesions: Six-month clinical and angiographic follow-up results of the APPLAUSE trial. *J Invasive Cardiol* 18:194–198.
28. Soppimath KS, Aminabhavi TM, Kulkarni AR, Rudzinski WE (2001) Biodegradable polymeric nanoparticles as drug delivery devices. *J Control Release* 70:1–20.
29. Alexis F, Pridgen E, Molnar LK, Farokhzad OC (2008) Factors affecting the clearance and biodistribution of polymeric nanoparticles. *Mol Pharm* 5:505–515.
30. Fishbein I, et al. (2001) Formulation and delivery mode affect disposition and activity of tyrphostin-loaded nanoparticles in the rat carotid model. *Arterioscler Thromb Vasc Biol* 21:1434–1439.
31. Decuzzi P, Ferrari M (2006) The adhesive strength of non-spherical particles mediated by specific interactions. *Biomaterials* 27:5307–5314.
32. Westedt U, et al. (2002) Deposition of nanoparticles in the arterial vessel by porous balloon catheters: Localization by confocal laser scanning microscopy and transmission electron microscopy. *AAPS PharmSci* 4:206–211.